A Framework for Robust Steady-State Voltage Stability of Distribution Systems

Hung D. Nguyen*, Krishnamurthy Dvijotham*, Suhyoun Yu, and Konstantin Turitsyn

Abstract—**Power distribution system's security is often jeopardized by network uncertainties, usually caused by the recent increase in intermittent power injections from renewable energy sources, and non-traditional energy demands. Naturally, there is an ever increasing need for a tool for assessing distribution system security. This paper presents a fast and reliable tool for constructing *inner approximations* of steady state voltage stability regions in multidimensional injection space such that every point in our constructed region is guaranteed to be solvable. Numerical simulations demonstrate that our approach outperforms all existing inner approximation methods in most cases. Furthermore, the constructed regions are shown to cover substantial fractions of the true voltage stability region. The paper will later discuss a number of important applications of the proposed technique, including fast screening for viable injection changes, constructing an effective solvability index and rigorously certified loadability limits.**

Index Terms—**Inner approximation, power flow, solvability, voltage stability,**

I. INTRODUCTION

Power distribution system's security is often threatened by network uncertainties. Often induced by intermittent distributed renewable energy resources or smart flexible loads, uncertainties are responsible for altering the system operating condition. A network that is forced to operate under unfavorable conditions may eventually be pushed out of its viable region where its steady-state equilibrium ceases to exist [1], [2], then experience instability, and finally fail altogether with a potential voltage collapse. Before proceeding further, we would like to address that while the two terms, "stability" and "security", in power system analysis may be technically distinct in definition, we would like to seek a pardon for abusing terminology by using "security", "stability", "viability", and "solvability" interchangeably.

The solution of power flow problem plays a critical role in steady state stability assessment by being the very indicator of the network's solvability. Disappearance of solutions, in turn, implies that the given injection, or the operating point, is beyond the network's solvability limit; that is, the network is incapable of supporting the amount of demanded load. Consequently, it is crucial for network security that power

Krishnamurthy Dvijotham is with the Department of Mathematics, Washington State University and with the Optimization and Control group, Pacific Northwest National Laboratory, Richland, WA 99354, USA email: dvij@cs.washington.edu.

Hung D. Nguyen, Suhyoun Yu, and Konstantin Turitsyn are with the Department of Mechanical Engineering, Massachusetts Institute of Technology, Cambridge, MA, 02139 USA e-mail: hungtd@mit.edu, syu2@mit.edu, and turitsyn@mit.edu.

* The first two authors contributed equally to this work.

system operators are aware of allowed ranges, or security regions, wherein the injections may vary without jeopardizing system stability. A security region is defined as the set of all viable injections, and this region may be useful for a number of power system operation and planning applications, including online security monitoring, corrective scheduling, and expansion planning [3].

Meanwhile, characterizing the security region is theoretically and computationally challenging due to the non-linearity of the power flow equations. In case of large scale systems, constructing a complete solvability regions is impossible with the only methods that are currently available. Moreover, it has been observed that the true solvability region may not necessarily be convex [4], [5], posing an even harsher challenge for online security-constrained functions.

To alleviate the computational burden of power-flow security analysis, we developed an analytic framework to constructs an inner approximation within the solvability region. Having a simple analytic form composed of norm constraints on an affine function of inputs, the structure of the developed framework has significant computational advantages, and we outline several applications of our technique to power systems that exploit the simple nature of the regions we construct. We demonstrate tightness of the solvability regions in the sense that our regions almost "touch" the boundary of the true, usually nonconvex, feasibility set.

The main contributions of the paper are as follows. In section III, we present our main technical contribution; in particular the sufficient condition for solvability of AC power flow equations appearing in a single-phase distribution system (not necessarily radial) with PQ buses only. The solvability condition allows one to construct inner approximations of the solvability region in multidimensional injection space. Section IV discusses a number of practical applications of our result: a fast screening technique for speeding up steady state stability analysis; develop a fast-to-compute and informative index for solvability; rigorous techniques for computing certified loading gain limits. Finally, in section V, we illustrate our technique's performance by testing on multiple IEEE distribution test feeders using MATPOWER.

A. Literature review

The steady state solvability of power systems has been studied for several decades. A review of literature in this problem can be found in [6]–[9]. The traditional method of assessing the system solvability involves solving the power flow equations numerically using a continuation method [10].

While these methods are theoretically ideal, practical implementations of these methods are limited due to the high computational burden; the conventional continuation methods are useful for tracing along a single given direction, but constructing a complete solvability boundary in all dimensions is next to being impossible. In contrast, analytic approaches provide an alternative solution with significantly lower computational burden, thus being more efficient and appropriate approach for time-sensitive tasks.

Analytic methods can be used to certify voltage stability of a single configuration of injections (point-wise certificates [11]–[13]) or for a set of injections (region-wise certificates [3], [14]–[16]). Several advantages of the latter have been discussed in [6], including less computational costs and the ability to provide security measures.

Unfortunately, most region-wise approaches suffer from conservatism in which the characterized sets can become overly small. In recent work, Banach's fixed point theorem has been successfully applied to distribution systems and shown to construct large subsets of the stability region [8], [9], [17]. Among these, the results presented in [9] (denoted WBBP in our paper based on the authors' last names) dominate all previous results. However, the WBBP's solvability criterion requires a specific condition on the nominal point around which the solvability region approximation is constructed. In the regime where this condition is close to being violated, the estimated regions become conservative as shown in section V-C.

In this work, we propose to use Brouwer's fixed point theorem—a popular fixed point theorem (especially in market economics [18])—to overcome the conservative nature of previous methods introduced above. The simulation results show that our estimated regions can cover up to 80% of the true solvability, thus being sufficiently large for operational purposes, and in most of cases, our approximation dominates WBBP's results. Moreover, while Simpson-Porco *et al.* have applied Brouwer's fixed point theorem to lossless radial networks in his recent work [19], our approach considers full AC power flow equations which describe the actual lossy systems.

In the scope of this paper, we only consider distribution systems with constant power PQ buses, and we neglect shunt elements, tap changers, switching capacitor banks and other discrete controls on the grid. Though it is possible to incorporate a simple bound on the voltage magnitudes, we do not aim to enforce operational constraints. Finally, the topology of the system is assumed to be unchanged; we do not consider contingencies involving transmission line losses. All extensions mentioned above are left for future research.

II. BACKGROUND AND NOTATION

The following notations will be used throughout this paper:

$\mathbb{C}$: Set of complex numbers

$[\![\boldsymbol{x}]\!] = \operatorname{diag}(\boldsymbol{x})$ for $\boldsymbol{x} \in \mathbb{C}^n, \overline{\boldsymbol{x}}$: Conjugate of $\boldsymbol{x} \in \mathbb{C}^n$

$\mathbf{1}$: Vector of compatible size with all entries equal to 1

$\mathbf{I}$: Identity matrix of compatible size

$$\|\boldsymbol{x}\| = \|\boldsymbol{x}\|_\infty = \max_i x_i \text{ for } \boldsymbol{x} \in \mathbb{C}^n$$

$$\|\boldsymbol{A}\| = \|\boldsymbol{A}\|_\infty = \max_i \sum_j |A_{ij}| \text{ for } \boldsymbol{A} \in \mathbb{C}^{n \times n}$$

$$\frac{\partial F}{\partial x} = \begin{pmatrix} \frac{\partial F_1}{\partial x_1} & \cdots & \frac{\partial F_n}{\partial x_1} \\ \vdots & \vdots & \vdots \\ \frac{\partial F_n}{\partial x_1} & \cdots & \frac{\partial F_n}{\partial x_n} \end{pmatrix} \text{ for } F : \mathbb{C}^n \mapsto \mathbb{C}^n$$

We study a power grid with one bus being the slack bus and all other buses modeled as PQ buses. We use 0 to denote the slack bus and $1, \ldots, n$ to denote the PQ buses. The slack bus voltage V_0 will be fixed as a reference value, and $V_1, \ldots, V_n$ are variables. The complex net power injection at bus i will be denoted as $s_i = p_i + \mathbf{j}q_i$, where p_i is the active power injection and q_i is the reactive power injection. The sub-matrix of the admittance matrix corresponding to the PQ buses can be constructed by eliminating the first row and column, and this sub admittance matrix will be denoted by $\mathbf{Y} \in \mathbb{C}^{n \times n}$ and its (i, k)-th entry as Y_{ik}. The power balance equations can then be written as

$$\overline{Y_{i0}}V_i\overline{V_0} + \sum_{k=1}^n \overline{Y_{ik}}V_i\overline{V_k} = s_i = p_i + \mathbf{j}q_i, \quad i = 1, \ldots, n.$$

Let V^0 denote the voltage solution corresponding to the zero injection and zero current condition. V^0 is the solution to the system of linear equations

$$\sum_{k=1}^n \overline{Y_{ik}}V_i^0 + \overline{Y_{i0}}V_0 = 0, \quad i = 1, \ldots, n.$$

The power-flow equations can then be expressed in the following compact form:

$$[\![\boldsymbol{V}]\!]\overline{\boldsymbol{Y}(\boldsymbol{V} - \boldsymbol{V^0})} = \boldsymbol{s} \tag{1}$$

Theorem 1 (Brouwer's fixed point theorem [20]): Let $F : \mathbb{C}^n \mapsto \mathbb{C}^n$ be a continuous function. Suppose that there is a convex set $S \subseteq \mathbb{C}^n$ such that

$$F(\boldsymbol{x}) \in S \quad \forall \boldsymbol{x} \in S,$$

then $F(\boldsymbol{x}) = \boldsymbol{x}$ has a solution in S.

We will use this theorem to derive sufficient conditions on $\boldsymbol{s}$ so that the conditions guarantee the existence of solutions to the power flow equations. Note that there are similar results for more general sets of quadratic equations have been reported in our recent work [21].

III. SOLVABILITY CERTIFICATES

In this section, we will apply Brouwer's fixed point theorem to the full AC power flow equations in (1). The central result for the existence of a steady state solution is introduced below.

Theorem 2: Let $(\boldsymbol{V}_\star, \boldsymbol{s}_\star)$ be any solution to the power flow equations (1). Define

$$\boldsymbol{Z}_\star = [\![\,\overline{\boldsymbol{V}_\star}\,]\!]^{-1} \overline{\boldsymbol{Y}}^{-1} [\![\,\boldsymbol{V}_\star\,]\!]^{-1} \tag{2a}$$

$$\boldsymbol{J}_\star = \begin{pmatrix} \mathbf{I} & \overline{\boldsymbol{Z}_\star}[\![\,\overline{\boldsymbol{s}_\star}\,]\!] \\ \boldsymbol{Z}_\star[\![\,\boldsymbol{s}_\star\,]\!] & \mathbf{I} \end{pmatrix} \tag{2b}$$

$$(\boldsymbol{J}_\star)^{-1} = \begin{pmatrix} \boldsymbol{M}_\star & \boldsymbol{N}_\star \\ \overline{\boldsymbol{N}_\star} & \overline{\boldsymbol{M}_\star} \end{pmatrix} \tag{2c}$$

where $\boldsymbol{J}_\star$ is nonsingular. Let $\boldsymbol{s} \in \mathbb{C}^n, r > 0$ be arbitrary and define $\Delta\boldsymbol{s} = \boldsymbol{s} - \boldsymbol{s}_\star$. Then, (1) has a solution if

$$\frac{1}{r}\left\| \boldsymbol{M}_\star \overline{\boldsymbol{Z}}_\star \overline{\Delta\boldsymbol{s}} + \boldsymbol{N}_\star \boldsymbol{Z}_\star (\Delta\boldsymbol{s}) \right\| + \left\| \boldsymbol{J}_\star^{-1} \right\| \left\| \boldsymbol{Z}_\star[\![\,\boldsymbol{s}\,]\!] \right\| r$$
$$+ \left\| \boldsymbol{M}_\star \overline{\boldsymbol{Z}_\star}[\![\,\overline{\Delta\boldsymbol{s}}\,]\!] + \boldsymbol{N}_\star[\![\,\boldsymbol{Z}_\star (\Delta\boldsymbol{s})\,]\!] \right\|$$
$$+ \left\| \boldsymbol{M}_\star[\![\,\overline{\boldsymbol{Z}_\star (\Delta\boldsymbol{s})}\,]\!] + \boldsymbol{N}_\star \boldsymbol{Z}_\star[\![\,\Delta\boldsymbol{s}\,]\!] \right\| \le 1 \tag{3}$$

Further, if $r < 1$, the solution V lies in the set

$$\frac{|V_{\star i}|}{1+r} \le |V_i| \le \frac{|V_{\star i}|}{1-r} \tag{4}$$

Proof 1: Define

$$\zeta(\boldsymbol{s}) = \overline{\boldsymbol{Z}_\star}[\![\,\overline{\boldsymbol{s}}\,]\!], \eta(\boldsymbol{s}) = \overline{\boldsymbol{Z}_\star \boldsymbol{s}}$$

Using lemma 1 in the Appendix, we can rewrite (1) as

$$\boldsymbol{y} + \zeta(\boldsymbol{s}_\star)\overline{\boldsymbol{y}} = -\eta(\Delta\boldsymbol{s}) - [\![\,\eta(\Delta\boldsymbol{s})\,]\!]\boldsymbol{y} - \zeta(\Delta\boldsymbol{s})\overline{\boldsymbol{y}}$$
$$- [\![\,\boldsymbol{y}\,]\!]\zeta(\boldsymbol{s})\overline{\boldsymbol{y}} \tag{5}$$

where $\boldsymbol{y} = \frac{\boldsymbol{V}_\star}{\boldsymbol{V}} - \mathbf{1}$, and $\frac{\boldsymbol{V}_\star}{\boldsymbol{V}}$ is the component-wise division of $\boldsymbol{V}_\star$ and $\boldsymbol{V}$. Let $\boldsymbol{\alpha}$ denote the LHS. We then have

$$\begin{pmatrix} \boldsymbol{\alpha} \\ \overline{\boldsymbol{\alpha}} \end{pmatrix} = \begin{pmatrix} \mathbf{I} & \overline{\boldsymbol{Z}_\star}[\![\,\overline{\boldsymbol{s}_\star}\,]\!] \\ \boldsymbol{Z}_\star[\![\,\boldsymbol{s}_\star\,]\!] & \mathbf{I} \end{pmatrix} \begin{pmatrix} \boldsymbol{y} \\ \overline{\boldsymbol{y}} \end{pmatrix}$$

so that

$$\boldsymbol{J}_\star^{-1} \begin{pmatrix} \boldsymbol{\alpha} \\ \overline{\boldsymbol{\alpha}} \end{pmatrix} = \begin{pmatrix} \boldsymbol{y} \\ \overline{\boldsymbol{y}} \end{pmatrix}$$

Then, (5) can be rewritten as

$$\boldsymbol{y} = -\left(\boldsymbol{M}_\star \eta(\Delta\boldsymbol{s}) + \boldsymbol{N}_\star \overline{\eta(\Delta\boldsymbol{s})} \right)$$
$$- \left(\boldsymbol{M}_\star[\![\,\boldsymbol{y}\,]\!]\zeta(\boldsymbol{s})\overline{\boldsymbol{y}} + \boldsymbol{N}_\star[\![\,\overline{\boldsymbol{y}}\,]\!]\overline{\zeta(\boldsymbol{s})}\boldsymbol{y} \right)$$
$$- \left(\boldsymbol{M}_\star[\![\,\eta(\Delta\boldsymbol{s})\,]\!] + \boldsymbol{N}_\star \overline{\zeta(\Delta\boldsymbol{s})} \right)\boldsymbol{y}$$
$$- \left(\boldsymbol{M}_\star \zeta(\Delta\boldsymbol{s}) + \boldsymbol{N}_\star[\![\,\overline{\eta(\Delta\boldsymbol{s})}\,]\!] \right)\overline{\boldsymbol{y}} \tag{6}$$

We apply Brouwer's fixed point theorem to (6) with the set $\{\boldsymbol{y} : \|\boldsymbol{y}\| \le r\}$. We take the norm of the RHS of (6) and apply triangle inequality and the definition of the matrix norm to obtain:

$$\left\| \boldsymbol{M}_\star \eta(\Delta\boldsymbol{s}) + \boldsymbol{N}_\star \overline{\eta(\Delta\boldsymbol{s})} \right\| + (\|\boldsymbol{M}_\star\| + \|\boldsymbol{N}_\star\|)\|\zeta(\boldsymbol{s})\| r^2$$
$$+ \left\| \boldsymbol{M}_\star \zeta(\Delta\boldsymbol{s}) + \boldsymbol{N}_\star[\![\,\overline{\eta(\Delta\boldsymbol{s})}\,]\!] \right\| r$$
$$+ \left\| \boldsymbol{M}_\star[\![\,\eta(\Delta\boldsymbol{s})\,]\!] + \boldsymbol{N}_\star \overline{\zeta(\Delta\boldsymbol{s})} \right\| r \tag{7}$$

Since (7) is an upper bound on the norm of the RHS of (6), Brouwer's fixed point theorem guarantees that (6) has

a solution if (7) is smaller than r. Dividing (7) by r and requiring the result to be smaller than 1, we obtain (3) which establishes the theorem. Moreover, the solution will exist in the set $\left\| \frac{\boldsymbol{V}_\star}{\boldsymbol{V}} - 1 \right\| \le r$, or

$$\left| \frac{V_{\star i}}{V_i} - 1 \right| \le r \implies |V_{\star i} - V_i| \le r|V_i|$$

Applying the triangle inequality, we obtain $|V_{\star i}| - |V_i| \le r|V_i|, |V_i| - |V_{\star i}| \le r|V_i|$ or

$$\frac{|V_{\star i}|}{1+r} \le |V_i| \le \frac{|V_{\star i}|}{1-r} \tag{8}$$

The solvability condition presented in (3) is particularly useful if one is seeking for a solution that lies within some voltage bounds characterized by r. The value of r reflects the size of the solvability region; hence if one's focus is on solvability of given injections, then one might be interested in finding the largest possible estimated subsets, which can be found by optimizing the value of r, thus directing to the following result.

Corollary 1: Let S_r denote the set of s satisfying (3). Define the set

$$\mathcal{S}_r = \cup_{0 < \epsilon \le 1} S_{\epsilon r}$$

Then, for every $\boldsymbol{s} \in \mathcal{S}_r$, there exists a solution $\boldsymbol{V}$ to (1) satisfying (4). Further, for every $\boldsymbol{s}$ satisfying

$$2\sqrt{\left\| \boldsymbol{M}_\star \overline{\boldsymbol{Z}_\star}[\![\,\overline{\Delta\boldsymbol{s}}\,]\!] + \boldsymbol{N}_\star \boldsymbol{Z}_\star[\![\,\Delta\boldsymbol{s}\,]\!] \right\| \left\| \boldsymbol{J}_\star^{-1} \right\| \left\| \boldsymbol{Z}_\star[\![\,\boldsymbol{s}\,]\!] \right\|}$$
$$+ \left\| \boldsymbol{M}_\star \overline{\boldsymbol{Z}_\star}[\![\,\overline{\Delta\boldsymbol{s}}\,]\!] + \boldsymbol{N}_\star[\![\,\boldsymbol{Z}_\star (\Delta\boldsymbol{s})\,]\!] \right\|$$
$$+ \left\| \boldsymbol{M}_\star[\![\,\overline{\boldsymbol{Z}_\star (\Delta\boldsymbol{s})}\,]\!] + \boldsymbol{N}_\star \boldsymbol{Z}_\star[\![\,\Delta\boldsymbol{s}\,]\!] \right\| \le 1 \tag{9}$$

there is a solution $\boldsymbol{V}$ to (1). It can be seen that $\mathcal{S}_r$ is indeed the union of all $\mathcal{S}_{r'}$ where $0 \le r' \le r$. In other words, for more restricted range of voltage solutions, the corresponding subset $\mathcal{S}_{r'}$ will be contained in the subset $\mathcal{S}_r$. Note that, given a zero-loading nominal point, if it satisfies our certificate (9) then it also satisfies the certificate by WBBP, so our estimated regions will be guaranteed to contain those produced by WBBP's method. The theoretical comparison is presented in detail in [21].

One of the most important potential applications of the inner approximation technique is that the solvable subsets can replace the power flow constraints in a security-constrained optimization function. The new optimization problem then does not require to solve the power flow equations directly; instead it searches for the optimal injection inside the solvability subsets which are in parameter spaces. Meanwhile, in order to take advantage of convex optimization, we further modified the solvable sets to take a convex representation with the corollary below.

Corollary 2: The set defined by constraint (3) is convex; in particular, it can be represented as the feasible subset of a second order conic program (SOCP).

Proof 2: Since $|\boldsymbol{x}| = \sqrt{\Re(\boldsymbol{x})^2 + \Im(\boldsymbol{x})^2}$, the constraint $|\boldsymbol{x}| \le t$ is equivalent to $\left\| \begin{pmatrix} \Re(\boldsymbol{x}) \\ \Im(\boldsymbol{x}) \end{pmatrix} \right\|_2 \le t$ which is a second order cone constraint. Since all the terms in the constraint (3) has the ∞ norm of a complex vector $\boldsymbol{x}$ (which is $\max_i |x_i|$) or

a complex matrix $\boldsymbol{X}$ (which is $\max_i \sum_j |X_{ij}|$), the condition (3) can be represented as a set of SOCP constraints.

IV. APPLICATIONS

The proposed sufficient solvablity criteria are useful for a number of important operational functions including, but not limited to, verifying viable injections, loadability limit monitoring, and security-constrained optimization functions. As discussed at the end of section III, it is possible to construct approximated convex regions which each has a simple analytic form. Such convex shapes then can be incorporated into the constrained optimization by replacing the original nonlinear power flow equations. Nevertheless, in the scope of this paper, we only consider three immediate applications: fast screening for viable injection change, effective solvability index, and certified loadability limit estimation.

A. Fast screening for viable injection change

The verification problem mainly concerns whether an injection is viable or not. Carrying out the verification over the real solvability region is challenging because the actual boundary is difficult to construct. Alternatively, we propose to use the approximated region characterized by sufficient solvability criteria. If the approximated solvability region is convex, the verification problem is indeed a membership oracle, a basic algorithmic convex geometry problem [22]. Once an injection is verified, the corresponding operating point is guaranteed to be solvable. Otherwise, other detailed tests need to take place. For fast screening purposes, we introduce a speeding up algorithm below.

The screening problem usually considers a cloud of points in the injection space, so-called the potential injection set, and the task is to classify all solvable and unsolvable points to sets $\mathcal{F}$ and $\mathcal{I}$, respectively. A fast screening procedure is presented in Algorithm 1. In the proposed algorithm, power flow (PF) (or continuation power flow (CPF) if PF does not converge) only needs to perform for the candidate scenario, the so-called seed point. If any point in the given potential injection set satisfies the solvability condition (9) associated with the seed point, it is certified as solvable. Among uncertified points which may or may not be solvable, we select another seed point and continue the screening process until all points from the potential injection set are classified.

In contrast, a traditional screening procedure needs to solve PF or CPF for each scenario in set $\mathcal{P}$ to determine its solvability. Figure 1 illustrates the performance of the fast screening algorithm against a CPF-based one in terms of elapsed time. In this simulation, the potential injection set is generated uniformly randomly which mimics uncertain renewable injections. As expected, the time acceleration factor tends to increase when more scenarios are considered. The simulation results show that the proposed method can speed up the screening up to 400 times. According to our numerical observation, the performance of the fast screening method depends on the density of the potential injection set. The more concentrated the potential injection points are, the faster the screening outperforms.

Algorithm 1 Fast screening algorithm based on Brouwer's theorem

1: Store all potential injections in a set $\mathcal{P}$
2: Initialize a set $\mathcal{I}$ and $\mathcal{F}$ as an empty set
3: **While** $\mathcal{P}$ is not empty **do**
  • Choose the first point as a seed
  • Solve PF (or CPF) for the seed and remove the seed from $\mathcal{P}$
    if solvable **then**
      add the seed to $\mathcal{F}$
      for $i = 1, \cdots, \text{card}(\mathcal{P})$ **do**
        if $\mathcal{P}(i)$ satisfies (9) w.r.t the seed **then**
          remove $\mathcal{P}(i)$ from $\mathcal{P}$ and add it to **F**
        end if
      end for
    else
      add the seed to $\mathcal{I}$
    end if
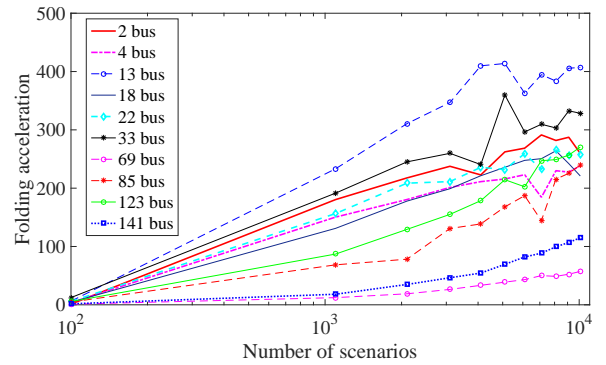4: Return $\mathcal{I}$ and $\mathcal{F}$

Fig. 1: The performance of the fast screening algorithm against a CPF-based approach

B. Effective solvability index

The above fast screening needs to verify all potential injection points by constructing multiple certificates; the proceeding section demonstrates the effectiveness of a single certificate by constructing the solvability region and calculating the percentage of certified points, or equivalently, the percentage of points that lie inside the constructed region. This percentage can serve as an estimated measure of solvability, so-called effective solvability index, which can help the system operators to quickly make decisions on whether or not to continue operating the system (with the same settings) under a given level of uncertainty of power injections. An example of the procedure calculating the index is described below.

Figure 2 illustrates the performance, in terms of the percentage of certified random injections, of a single certificate characterized by (9) for several IEEE distribution test feeders with renewables. We modify the test cases to accommodate ∼35% renewable penetration by installing photovoltaic panels (PVs) at more than one third of the load buses. The PV locations are selected uniformly and randomly. Potential injection sets are generated by varying the PV outputs with
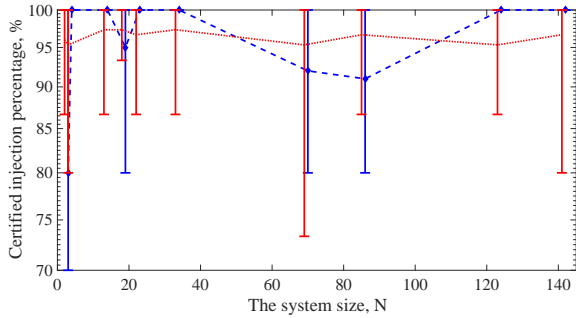
Fig. 2: The effective solvability index

two separate methods; the first method randomly selects PV outputs from a uniform distribution over a range of $\pm 500\%$ of the base load/injection, while the second method randomly and uniformly selects from the forecast data for May 03, 2017 available online [23]. In Figure 2, the results were recorded in the percentage of number of injections certified, where the red and blue data corresponds to the first and second PV output selection methods, respectively.

As indicated in the plot, one single certificate, on average, is able to certify $\sim 95\%$ of the random injection sets, and even the lower bound of this percentage is well over the majority. For all test cases, it is also evident that the certificate may even extend to certify exhaustively the potential sets. The simulation thus illustrates that even with the high uncertainty and randomness added from the renewable injections, one certificate can encompass a considerable portion of the solvability region. Apparently, though the performance of one certificate might depend on the test case configurations as well as the random injection sets, the operators can carry out this quick test to roughly estimate the system viability for a given amount of uncertain injections. If the index above an acceptable level of security, say 0.95, no more assessment is required.

C. Certified admissible gain limits

In practice, the system operators may be interested in the distance between the current operating point and the insolvable boundaries. If the loading direction and the aspect ratio are fixed, one can solve for the maximum incremental gain, λ_{max}, for which the system remains solvable. The smallest λ_{max} of all possible loading directions—or the so-called loading gain limit—can also be used to quantify the system stability. Solving for the loading gain limit can be formulated as a $\min - \max$ optimization problem described below:

$$\min_{\Delta u} \ \max_{\lambda} \ \lambda \qquad (10)$$
$$\text{subject to} \quad s_\star + \lambda \Delta u \text{ is solvable,}$$
$$0 \le \lambda, \|\Delta u\| = 1$$

where Δu is the normalized vector that represents a possible loading direction. The optimization problem (10) is difficult to solve in general; however, solvability condition (9) can estimate a lower bound called the certified admissible gain, λ_{CAG}.

System size, N	λ_{CAG}/λ_R	λ_{CAG}/λ_B
3	0.7456	0.9507
18	0.4102	0.6173
33	0.5084	0.6629
69	0.3123	0.4080
123	0.5759	0.7708

TABLE I: Certified gain limits vs. the estimated and true ones

To find the certified gain limit, we introduce a stronger form of (9):

$$2\sqrt{\left(\left\|M_\star \overline{Z}_\star\right\| + \|N_\star Z_\star\|\right)\left\|J_\star^{-1}\right\| \|Z_\star\| \lambda \left(\|s_\star\| + \lambda\right)}$$
$$+ 2\left(\left\|M_\star \overline{Z}_\star\right\| + \|N_\star Z_\star\|\right) \lambda \le 1. \qquad (11)$$

The triangle inequality verifies that any variation $\Delta s = \lambda \Delta u$ that satisfies (11) will also satisfy (9). Let the inequality (11) hold as an equality, and let λ_M be the larger positive root of the corresponding equation: then the certified admissible gain is defined as

$$\lambda_{CAG} = \min\{\lambda_M, 0.5/\left(\left\|M_\star \overline{Z}_\star\right\| + \|N_\star Z_\star\|\right)\}. \qquad (12)$$

The second argument under the operator $\min$ is necessary to guarantee the real non-negativity of the square root term in (11).

Note that the certified gain is indeed a "worst-case" loading gain which is unique for a base operating point and does not depend on the loading direction. For any normalized incremental loading direction Δu, the system is guaranteed to be safe from a voltage instability problem as long as the loading gain does not exceed λ_{CAG}. To validate the certified loading gain, we compare it with the estimated gain λ_B from condition (9) and the actual gain limit, λ_R. The loading direction is chosen such that all loads increase equally. This specific direction is one of the most dangerous directions along which the system soon becomes stressed and the stability margin decreases significantly. Table I shows that, for this dangerous loading direction, the certified gain is around $30\% - 80\%$ of the true gain limits. For the estimated gain from (9), the ratios are higher, or even equal to 1 in some cases. When the ratio reaches 1, the condition (9) and its strong form (11) are equivalent along the homogeneous loading direction.

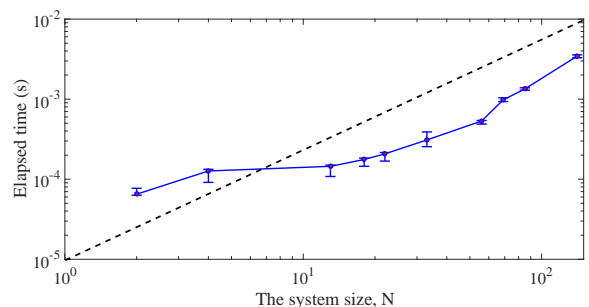## V. NUMERICAL STUDIES

A. Run-time analysis

Fig. 3: A log-log plot for computation time vs. the system size

For the proposed inner approximation technique, the main burden is to explicitly compute for the impedance matrix $\mathbf{Z}$, the inverse of the admittance matrix $\mathbf{Y} \in \mathbb{C}^{N \times N}$. In our framework, matrix $\mathbf{Z}$ may be computed only once unless the network topology changes. For a base operating point, the nominal matrix $\mathbf{J}_\star$ and its inverse are constant; therefore, they can be reused while repeatedly generating the certificate (9). A run-time analysis is performed to estimate the running time needed to generate a single certificate as the size of system, N, increases. In particular, for each test case, we repeatedly generate the same certificate and measure the corresponding elapse time. Empirical metrics recorded in Figure 3 shows that the time complexity is close to $O(N)$, implying that the run-time scales linearly with the system size.

B. A toy example and the coalescense condition

Consider a 2-bus test case with a slack bus with $V_0 = 1\angle 0$, and one load bus with unknown voltage $V\angle\theta$ consuming an amount of apparent power $S = P + jQ$. The line connecting the two buses has an impedance of $R + jX$. In the base case, we have $S_\star = 0$ and $V_\star = V_0$. Applying the condition (9) to the 2-bus system yields the inequality below:

$$\sqrt{(R^2 + X^2)(P^2 + Q^2)} \leq \frac{1}{4}. \qquad (13)$$

In the following simulations, we construct the estimated solvability boundaries and the real boundaries while varying the R/X ratio. Very high R/X ratios are not practical, yet we examine such extreme cases to illustrate the conditions for the coalescence between the approximated and the actual solvability boundaries. Figure 4 is plotted in PQ space

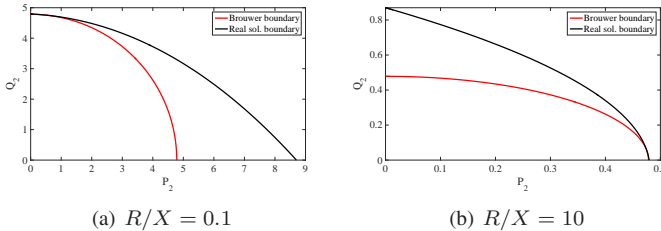(a) $R/X = 0.1$ (b) $R/X = 10$

Fig. 4: Solvability regions of a two-node test feeder for a zero base load and different R/X ratios

where the solid black curves represent the real boundaries, and the solid red curves represent the estimated boundaries using Brouwer approach. From Figure 4, the most important observation is that the two boundaries may be tight in some directions that satisfies the condition $P/Q = R/X$, a ratio which we will refer to as the "matching" ratio. Note that the equation $P/Q = \cot(\phi)$ holds, where $\cos(\phi)$ is the load power factor. The coalescence condition is then proved as below.

For the 2-bus toy system, the magnitude of the voltage solution, V, satisfies the following bi-quadratic equation:

$$V^2 = V^4 + 2(RP + XQ)V^2 + (R^2 + X^2)(P^2 + Q^2).$$

The condition for the existence of a real solution can be expressed as

$$(RP + XQ - \frac{1}{2})^2 - (R^2 + X^2)(P^2 + Q^2) \geq 0 \qquad (14)$$

which can be further simplified to

$$(RQ - XP)^2 + RP + XQ \leq \frac{1}{4}. \qquad (15)$$

Under the coalescence condition $\frac{R}{X} = \frac{P}{Q}$, both sufficient solvability condition (13) and the real condition (15) define the same solvability boundary characterized by $|RP + XQ| = \frac{1}{4}$.
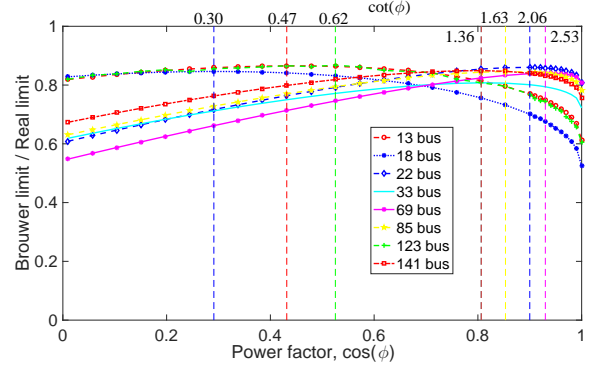

Fig. 5: Solvability regions comparisons with different power factors

Test feeder	Matching P/Q $\cot(\phi)$	Average R/X	Common R/X range
33-node	1.36	1.44	1.07-1.36
69-node	2.53	2.07	2.80-3.10
123-node	0.62	0.63	0.40-0.62
141-node	1.36	1.71	1.16-1.74

TABLE II: Coalescence condition: matching $P/Q - R/X$ ratios

The coalescence condition also holds for large scale distribution systems with a zero-loading base point. Figure 5 plots the covering ratio–which we define as the ratio of the estimated loadability limit to the real loadability limit–against the homogeneous power factors $\cos(\phi)$ as well as $\cot(\phi)$. The intersection point of each pair, consisting of the horizontal curve and the vertical line of the same colour, indicates the maximum ratio for the corresponding distribution system. All the maximum ratios are larger than 0.8, indicating that the estimated solvability limit can cover more than 80% of the actual limit. Moreover, the matching P/Q ratio or $\cot(\phi)$ can be approximated by the average R/X ratio of the lines. In all considered test cases, with $P/Q = \langle R/X \rangle$, the maximum covering percentage is circa 80%. It can also be seen that if the lines are almost homogeneous in terms of the R/X ratio, the matching ratio likely falls within the most common range of R/X as shown in Table II for the 33-node, 69-node, 123-node, and 141-node test feeders.

C. Large-scale distribution feeders

In this section, we continue constructing the solvability regions for larger scale test feeders. Some of those test cases
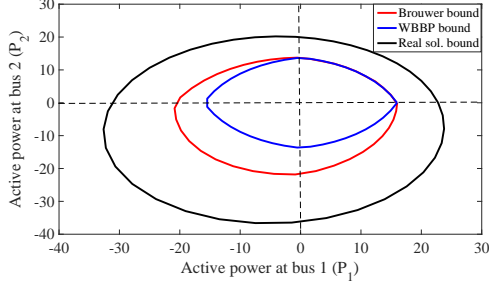
Fig. 6: Solvability regions of IEEE 123-node test feeder for a zero-loading base case
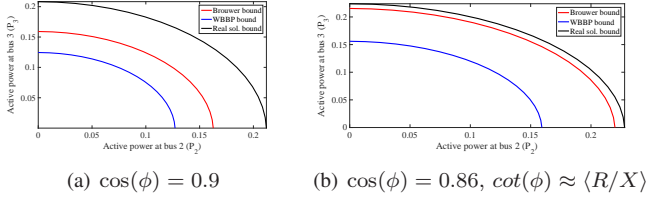

Fig. 8: Solvability regions of IEEE 141-node test feeder with different radii r of voltage bounds

(a) $\cos(\phi) = 0.9$ (b) $\cos(\phi) = 0.86$, $cot(\phi) \approx \langle R/X \rangle$

Fig. 7: Solvability regions of IEEE 141-node test feeder

(a) Brouwer's results are superior   (b) WBBP's results are superior

Fig. 9: Solvability regions of IEEE 123-node test feeder [25] for nonzero loading base cases

are provided in MATPOWER package [24]. Note that most of our simulations consider incremental loading scenarios which maintain a constant power factor of $\cos(\phi) = 0.9$. The effect of the power factor is discussed in section V-B. For a normal loading condition, Figures 6, 7 show that the approximated solvability region is large enough compared to the actual loadability region. Figure 7(b) illustrates the coalescence condition where the relation $P/Q \approx \langle R/X \rangle$ holds, implying that the estimated boundary almost matches the actual one. In addition, if the voltage bound of the solutions is of interest, one can construct the solvability region using (3) with the corresponding radius r where $0 \leq r < 1$. The volume of the union of the regions $\mathcal{S}_r$ increases with r, implying that, if one imposes a tighter bound on the voltage solution, then the power injections need also be confined inside a smaller set. Figure 8 clearly confirms the preceding statement.

We also compare our method with that of WBBP introduced in [9]. In most of the cases, the solvable regions constructed using Brouwer's approach encompass WBBP's. Figure 6 shows that for a zero-loading base point, our certificate is identical to WBBP's in the consumption regime, but it starts dominating as the loads inject powers. In practice, the injecting condition can be realized with distributed generation. There are some special cases, for instance: in Figure 9(a), Brouwer boundary is much larger than that of WBBP's. In this particular simulation, the load consumes more reactive power than active power at the base operating point. From a mathematical perspective, such base point voltage is close to the limit where WBBP's solvability condition is no longer valid. As a result, the characterized region becomes extremely conservative. In contrast, our estimation is still functional. However, there exist some regimes where WBBP's method outperforms ours. An example of such cases is shown in Figure 9(b) where the system is much more stressed than usual.
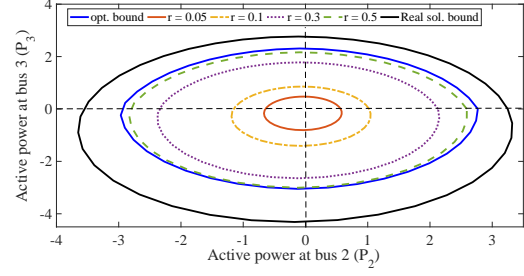
The relative performance comparison between the two methods is extensively analyzed for the modified 141-node test feeder with renewable penetration used in section IV-B. We assess $10,000$ random loading scenarios in which the load buses with PVs can either inject or consume powers. The histograms plotted in Figure 10 shows that WBBP's results can cover circa 80% of ours, which in turn cover almost the same percentage of the real limits.

VI. CONCLUSIONS AND FUTURE WORK

In this paper, we developed an inner approximation technique for constructing convex subsets of the solvability region for distribution systems based on Brouwer's fixed point theorem. The constructed regions can be used in security-related functions that rely on steady state snapshots. In particular, the proposed fast screening tool based on the sufficient solvability conditions was shown to have a considerably faster screening process compared to that of the conventional screening process. Meanwhile, we introduced a new stability indicator, the certified admissible gain limit, which represents a safe gain wherein the system may move along any incremental loading directions without exhibiting voltage instability.

(a) WBBP's/Brouwer's limit ratio   (b) Brouwer's/Real limit ratio
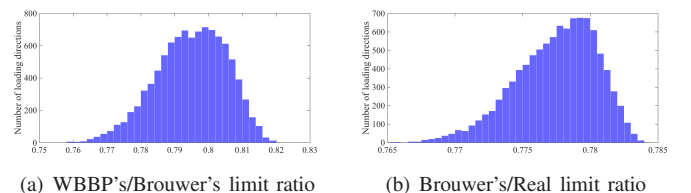
Fig. 10: Comparison of WBBP's, Brouwer's, and real loading limits for IEEE 141-node test feeder

As mentioned earlier, this work focuses only on distribution systems with PQ loads, and only simple bounds on the voltage solution can be imposed. For future research, we plan to extend the proposed technique to handle voltage-controlled buses in transmission networks and incorporate operational constraints such as voltage and current limits. In addition, it is possible to include 3-phase AC distribution systems in the proposed framework.

VII. Acknowledgement

References

[1] T. J. Overbye, "A power flow measure for unsolvable cases," *Power Systems, IEEE Transactions on*, vol. 9, no. 3, pp. 1359–1365, 1994.

[2] T. J. Overbye, "Computation of a practical method to restore power flow solvability," *Power Systems, IEEE Transactions on*, vol. 10, no. 1, pp. 280–287, 1995.

[3] F. C. S. E. Hnyilicza, S. T. Y. Lee, "Steady-state security regions: The set theoretic approach," *Proc. 1975 PICA Conf.*, pp. 347–355, 1975.

[4] I. A. Hiskens and R. J. Davy, "Exploring the power flow solution space boundary," *IEEE Transactions on Power Systems*, vol. 16, no. 3, pp. 389–395, Aug 2001.

[5] D. K. Molzahn, V. Dawar, B. C. Lesieutre, and C. L. DeMarco, "Sufficient conditions for power flow insolvability considering reactive power limited generators with applications to voltage stability margins," in *Bulk Power System Dynamics and Control-IX Optimization, Security and Control of the Emerging Power Grid (IREP), 2013 IREP Symposium*. IEEE, 2013, pp. 1–11.

[6] K. Loparo and F. Abdel-Malek, "A probabilistic approach to dynamic power system security," *IEEE transactions on circuits and systems*, vol. 37, no. 6, pp. 787–798, 1990.

[7] F. Wu and S. Kumagai, "Steady-state security regions of power systems," *IEEE Transactions on Circuits and Systems*, vol. 29, no. 11, pp. 703–711, Nov 1982.

[8] S. Bolognani and S. Zampieri, "On the existence and linear approximation of the power flow solution in power distribution networks," *IEEE Transactions on Power Systems*, vol. 31, no. 1, pp. 163–172, 2016.

[9] C. Wang, A. Bernstein, J.-Y. Le Boudec, and M. Paolone, "Existence and uniqueness of load-flow solutions in three-phase distribution networks," *IEEE Transactions on Power Systems*, 2016.

[10] Y. Zhou and V. Ajjarapu, "A fast algorithm for identification and tracing of voltage and oscillatory stability margin boundaries," *Proceedings of the IEEE*, vol. 93, no. 5, pp. 934–946, May 2005.

[11] D.-L. Tomas Enciso, "Control of power systems via the multi-level concept," 1968.

[12] A. Patton, "A probability method for bulk power system security assessment, i-basic concepts," *IEEE Transactions on Power Apparatus and Systems*, no. 1, pp. 54–61, 1972.

[13] L. Aolaritei, S. Bolognani, and F. Dörfler, "A distributed voltage stability margin for power distribution networks," *arXiv preprint arXiv:1612.00207*, 2016.

[14] M. Ilic-Spong, J. Thorp, and M. Spong, "Localized response performance of the decoupled q-v network," *IEEE transactions on circuits and systems*, vol. 33, no. 3, pp. 316–322, 1986.

[15] A. T. Saric and A. M. Stankovic, "Applications of ellipsoidal approximations to polyhedral sets in power system optimization," *IEEE Transactions on Power Systems*, vol. 23, no. 3, pp. 956–965, 2008.

[16] Y. V. Makarov, D. J. Hill, and Z.-Y. Dong, "Computation of bifurcation boundaries for power systems: a new δ-plane method," *Circuits and Systems I: Fundamental Theory and Applications, IEEE Transactions on*, vol. 47, no. 4, pp. 536–544, 2000.

[17] S. Yu, H. D. Nguyen, and K. S. Turitsyn, "Simple certificate of solvability of power flow equations for distribution systems," in *2015 IEEE Power Energy Society General Meeting*, July 2015, pp. 1–5.

[18] D. Gale, "The game of hex and the brouwer fixed-point theorem," *The American Mathematical Monthly*, vol. 86, no. 10, pp. 818–827, 1979.

[19] J. W. Simpson-Porco, "A theory of solvability for lossless power flow equations–part ii: Existence and uniqueness," *arXiv preprint arXiv:1701.02047*, 2017.

[20] L. E. J. Brouwer, "Über abbildung von mannigfaltigkeiten," *Mathematische Annalen*, vol. 71, no. 1, pp. 97–115, 1911.

[21] K. Dvijotham, H. Nguyen, and K. Turitsyn, "Solvability regions of affinely parameterized quadratic equations," *arXiv preprint arXiv:1703.08881*, 2017.

[22] S. S. Vempala, "Recent progress and open problems in algorithmic convex geometry," in *LIPIcs-Leibniz International Proceedings in Informatics*, vol. 8. Schloss Dagstuhl-Leibniz-Zentrum fuer Informatik, 2010.

[23] "Solar-pv generation forecasts." [Online]. Available: http://www.elia.be/en/grid-data/power-generation/Solar-power-generation-data/Graph

[24] "Matpower," 2017. [Online]. Available: https://github.com/MATPOWER/matpower

[25] S. Bolognani, "approx-pf-approximate linear solution of power flow equations in power distribution networks," 2014. [Online]. Available: http://github.com/saveriob/approx-pf

VIII. Appendix

Lemma 1: (1) can be rewritten as

$$\boldsymbol{y} + \zeta\left(\boldsymbol{s}_\star\right)\overline{\boldsymbol{y}} = -\eta\left(\Delta\boldsymbol{s}\right) - [\![\,\eta\left(\Delta\boldsymbol{s}\right)\,]\!]\boldsymbol{y} - \zeta\left(\Delta\boldsymbol{s}\right)\overline{\boldsymbol{y}} - [\![\,\boldsymbol{y}\,]\!]\zeta\left(\boldsymbol{s}\right)\overline{\boldsymbol{y}}$$

where $\boldsymbol{y} = \frac{\boldsymbol{V}_\star}{\boldsymbol{V}} - \mathbf{1}, \boldsymbol{\gamma}_\star = \frac{\boldsymbol{V}^0}{\boldsymbol{V}_\star}$.

Proof 3:

(1) can be rewritten as

$$\overline{\boldsymbol{Y}}^{-1}[\![\,\boldsymbol{V}\,]\!]^{-1}\boldsymbol{s} = \overline{\boldsymbol{V} - \boldsymbol{V}^0}.$$

Multiplying by $[\![\,\overline{\boldsymbol{V}}\,]\!]^{-1}$ on the left, we get

$$[\![\,\overline{\boldsymbol{V}}\,]\!]^{-1}\overline{\boldsymbol{Y}}^{-1}[\![\,\boldsymbol{V}\,]\!]^{-1}\boldsymbol{s} = \mathbf{1} - [\![\,\overline{\boldsymbol{V}}\,]\!]^{-1}\overline{\boldsymbol{V}^0}.$$

The above equation reduces to

$$[\![\,\boldsymbol{x}\,]\!]\left(\boldsymbol{Z}_\star[\![\,\boldsymbol{s}\,]\!]\overline{\boldsymbol{x}} + \overline{\boldsymbol{\gamma}_\star}\right) = \mathbf{1}$$

where $x = \overline{\left(\frac{\boldsymbol{V}_\star}{\boldsymbol{V}}\right)}$. Let $\boldsymbol{y} = \overline{\boldsymbol{x}} - \mathbf{1}$. Conjugating the above equation, we obtain

$$[\![\,\mathbf{1} + \boldsymbol{y}\,]\!]\left(\zeta\left(\boldsymbol{s}\right)\left(\mathbf{1} + \overline{\boldsymbol{y}}\right) + \boldsymbol{\gamma}_\star\right) = \mathbf{1}$$

which can be rewritten as

$$[\![\,\boldsymbol{y}\,]\!]\zeta\left(\boldsymbol{s}\right)\mathbf{1} + \zeta\left(\boldsymbol{s}\right)\overline{\boldsymbol{y}} + [\![\,\boldsymbol{y}\,]\!]\zeta\left(\boldsymbol{s}\right)\overline{\boldsymbol{y}} + [\![\,\boldsymbol{\gamma}_\star\,]\!]\boldsymbol{y} + \eta\left(\Delta\boldsymbol{s}\right) = 0$$

where we use the relation that $\eta\left(\Delta\boldsymbol{s}\right) = \zeta\left(\boldsymbol{s}\right)\mathbf{1} + \boldsymbol{\gamma}_\star - \mathbf{1}$. This can be rewritten as

$$[\![\,\eta\left(\boldsymbol{s}\right) + \boldsymbol{\gamma}_\star\,]\!]\boldsymbol{y} + \zeta\left(\boldsymbol{s}\right)\overline{\boldsymbol{y}} + [\![\,\boldsymbol{y}\,]\!]\zeta\left(\boldsymbol{s}\right)\overline{\boldsymbol{y}} + [\![\,\boldsymbol{\gamma}_\star\,]\!]\boldsymbol{y} + \eta\left(\Delta\boldsymbol{s}\right) = 0. \quad (16)$$

We have that

$$\begin{aligned}
\eta\left(\boldsymbol{s}_\star\right) + \boldsymbol{\gamma}_\star &= \overline{\boldsymbol{Z}_\star\boldsymbol{s}_\star} + [\![\,\boldsymbol{V}_\star\,]\!]^{-1}\boldsymbol{V}^0 \\
&= [\![\,\boldsymbol{V}_\star\,]\!]^{-1}\boldsymbol{Y}^{-1}\left([\![\,\overline{\boldsymbol{V}_\star}\,]\!]^{-1}\overline{\boldsymbol{s}_\star} + \boldsymbol{Y}\boldsymbol{V}^0\right) \\
&= [\![\,\boldsymbol{V}_\star\,]\!]^{-1}\boldsymbol{Y}^{-1}\left(\boldsymbol{Y}\boldsymbol{V}_\star\right) = \mathbf{1}.
\end{aligned}$$

Thus, (16) can be rewritten as

$$\boldsymbol{y} + \zeta\left(\boldsymbol{s}_\star\right)\overline{\boldsymbol{y}} = -\eta\left(\Delta\boldsymbol{s}\right) - [\![\,\eta\left(\Delta\boldsymbol{s}\right)\,]\!]\boldsymbol{y} - \zeta\left(\Delta\boldsymbol{s}\right)\overline{\boldsymbol{y}} - [\![\,\boldsymbol{y}\,]\!]\zeta\left(\boldsymbol{s}\right)\overline{\boldsymbol{y}}.$$

Q.E.D.